Fluctuation-induced constraints on the observation of unbinding in a confined complex fluid

F. Clarysse and C. J. Boulter
Department of Mathematics, Heriot-Watt University, Edinburgh EH14 4AS, United Kingdom
(Received 23 January 2001; published 25 June 2001)

An extensive study of the effect of fluctuations on the unbinding of an interface from a wall in a ternary system is presented. The framework upon which the analysis is based is a linear functional renormalization group scheme of the appropriate effective interface Hamiltonian. The interface model includes position-dependent gradient coefficients, and their presence is shown to be equivalent to modifications of the bare interface potential that are highly relevant in determining the renormalized critical behavior. We analyze the modified interface potential in a mean-field-like way for both bare critical and first-order unbinding transitions in order to highlight the key effects. We further perform a detailed study of the linearized renormalization group equations identifying three fluctuation regimes and recovering earlier predictions for nonuniversal critical exponents. The surface phase diagram changes dramatically under renormalization with, most notably, fluctuation-induced reentrant behavior. We show that in the revised phase diagram the unbound region is limited in extent indicating that the opportunity for observing an unbinding transition in a confined complex fluid is highly restricted.

DOI: 10.1103/PhysRevE.64.011604 PACS number(s): 68.08.Bc, 82.70.Uv, 05.70.Fh, 64.60.Fr

I. INTRODUCTION

There has been considerable recent interest in the chemistry and physics of complex fluids, mainly due to their wide range of applications and the diversity of structures that may be observed in these systems. The ubiquitous example is a ternary mixture of oil, water and surfactant or amphiphile for which the bulk phase behavior is well understood [1]. Furthermore, due to the potential coexistence of three or more bulk phases, these mixtures have attracted much attention from the point of view of interfacial critical phenomena and unbinding or wetting phase transitions [1–7].

In recent work we have focused on confined ternary systems and analyzed pure surface effects due to the presence of a wall or substrate [8–10]. More specifically, we have predicted the existence of an interface unbinding transition in a semi-infinite geometry at three-phase coexistence of the oil, water, and microemulsion. At this transition the wall-microemulsion interface is wetted by either the oil-rich or the water-rich phase. This study is based upon a Ginzburg-Landau (GL) free-energy functional of a single scalar order parameter $\phi(r)$ representing the local concentration difference between oil and water. The short-range wall-bulk interaction is accounted for via a surface density term,

$$\mathcal{L}_s = \mu_s \phi + \omega_s \phi^2 + g_s (\nabla \phi)^2, \tag{1.1}$$

which is characterized by three surface parameters. The parameter μ_s is the surface field or local chemical potential, while ω_s corresponds to the surface enhancement. Finally, the presence of a local gradient is essential for correctly determining the boundary conditions when using the simple GL theory, and the corresponding surface parameter g_s has been associated with the chemical potential of the amphiphile at the wall [7].

A powerful tool for studying unbinding transitions is an effective interface Hamiltonian, which is a functional of the thickness l of the adsorbed surface layer [11]. In contrast to the case of simple fluids where a standard square-gradient theory suffices, the appropriate model for ternary mixtures involves higher order gradient terms that are mostly justified on purely phenomenological grounds or derived from a simple rigid shift ansatz [12–14]. However, partly motivated by the failure of this approach to correctly describe a free oil-water interface (as demonstrated in [6]), a controlled and careful derivation of the Hamiltonian was recently presented, leading to an improved interface model for describing fluctuating interfaces and membranes in complex fluids [8–10]. The main new feature of the model is the presence of position-dependent stiffness and rigidity coefficients highly analogous to the discoveries of Fisher and Jin [15] and Fisher *et al.* [16] for wetting in simple fluids. Perhaps the most important ingredient of the model is the interfacial potential $W(l)$, the form of which fully determines the mean-field phase diagram. In particular, this is simply found by observing whether the global minimum of the potential is at a finite or infinite value of l, the first case referring to a bound state while in the latter the interface is said to be unbound from the wall.

The results of this mean-field analysis for the wall-microemulsion interface are best summarized by referring to Fig. 1, which is a schematic surface phase diagram as a function of the parameters μ_s and ω_s for fixed bulk parameters at three-phase coexistence. The generic behavior shown in the figure is not sensitive to the value of g_s. The diagram demonstrates that an unbinding transition can be induced either by increasing the absolute value of the surface field (which is assumed negative on physical grounds, see later), or by decreasing the value of the enhancement parameter ω_s. The transition is typically found to be first-order in the low $|\mu_s|$ regime [first-order (FW) wetting phase boundary], whereas for larger $|\mu_s|$ second-order or critical transitions are predicted [critical wetting (CW) phase boundary]. The two regimes are separated by a tricritical point (TCP) that is also the terminus for the two metastable limits associated with the

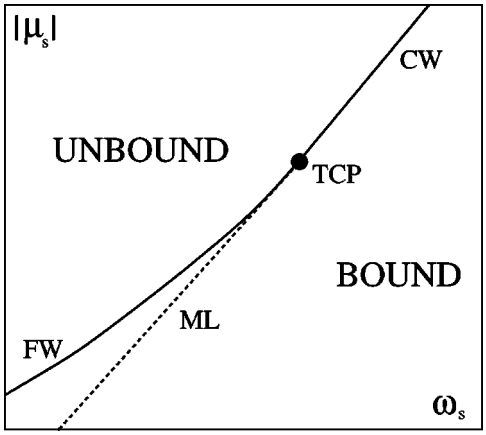

FIG. 1. Schematic mean-field phase diagram for the unbinding of a wall-microemulsion interface at bulk three-phase coexistence. First-order (FW) and continuous (CW) unbinding phase boundaries are shown by solid lines, and meet at the tricritical point (TCP). The dashed line ML denotes the metastable limit of the unbound state.

first-order transition [17]. For the unbound state, this metastable limit (ML) is given by the dashed line ML.

Experimental observations of the critical wetting transition predicted above are unlikely due to the presence of long-range van der Waals forces; however, in such systems a first-order transition is still predicted to be observable [9]. In contrast, Monte Carlo simulations may provide quantitative tests of the theoretical results for critical unbinding. Nevertheless, mean-field results are often a poor guide and at most qualitatively correct since they ignore the effect of fluctuations. Therefore it is important to ascertain the importance of thermally induced fluctuations on the overall phase behavior in complex fluids with short-range interactions. It is this issue we address in the present article.

We incorporate fluctuations by employing a linear functional renormalization group (RG) treatment of the effective interface model [15,18–20]. In this paper we apply the RG to provide a thorough understanding of the fluctuation effects. In particular, the position dependence of the gradient terms in the model proves to be highly relevant in determining the critical behavior, in analogy with the *instability mechanism* found for simple fluids, leading to critical transitions being driven fluctuation-induced first-order [21,20,22]. We demonstrate that for complex fluids the effect is even more drastic and gives rise to strong constraints on the possible observation of the unbinding transition in confined systems. Consequently, the mean-field phase diagram of Fig. 1 is significantly modified due to fluctuations and the revised phase diagram is one of our main results.

The remainder of the paper is organized as follows. In Sec. II we recall the main ingredients of the effective interface Hamiltonian for a ternary system with an external surface. We describe the generic expressions for both the interface potential and the gradient coefficients near critical unbinding and introduce the functional RG scheme for the model. This reveals that the presence of position-dependent gradient coefficients has the same effect as modifying the bare interface potential. In Sec. III we analyze the modified potential in a mean-field-like way near the critical transition, which provides a useful guide to the importance of the position-dependent gradient coefficients. Section IV deals with the fully linearized RG study based on a standard matching and rescaling procedure in the critical limit, from which we identify three scaling regimes. Results are presented for the various phase boundaries, the different singularities, and the critical exponents. In Sec. V we gauge the effect of fluctuations on the first-order boundary of Fig. 1 and assemble the results to sketch a renormalized phase diagram. This section also provides a summary of the implications of the RG theory for the phase behavior. We close the paper by discussing the relevance of our results for simulations and their applicability to other unbinding transitions in ternary systems.

II. INTERFACE MODEL AND FUNCTIONAL RENORMALIZATION

A. Background

The functional RG approach for wetting transitions is based on an effective interfacial Hamiltonian, $\mathcal{H}_l[l(\mathbf{y})]$, where $l(\mathbf{y})$ measures the distance of the interface from a wall, assumed to be in the plane $z=0$. With this notation $\mathbf{y}$ denotes the $(d-1)$-component vector specifying a point on the wall. This Hamiltonian may be derived systematically from the underlying bulk order-parameter theory by introducing a *crossing constraint* definition of the collective coordinate l and taking a trace over the remaining degrees of freedom [15,16,20]. This nontrivial formalism was recently implemented for ternary systems and the following Hamiltonian was obtained [8]

$$\mathcal{H}_l[l]=\int d\mathbf{y}\{\tfrac{1}{2}\kappa(l)(\nabla^2 l)^2+\tfrac{1}{2}\Sigma(l)(\nabla l)^2+W(l)\}. \tag{2.1}$$

We note that this Hamiltonian model is valid for any situation where there are interactions between two surfaces in a ternary amphiphilic system; however, we concentrate here on the case of an interface unbinding from a wall. We further assume three-phase coexistence with the middle or microemulsion phase stable in the bulk, i.e, in the limit $z\to\infty$, and a negative surface field μ_s such that the denser water phase is adsorbed by the substrate [23].

The interface potential $W(l)$, which describes the interaction of the interface with the wall, and the position-dependent *curvature* and *stiffness* coefficients, $\kappa(l)$ and $\Sigma(l)$ respectively, can be expressed in terms of the planar constrained order-parameter profile ϕ_π, full expressions are given in Ref. [9]. The gradient coefficients $\kappa(l)$ and $\Sigma(l)$ contain explicit l-dependent pieces, $\Delta\kappa(l)\equiv\kappa(l)-\kappa_\infty$ and $\Delta\Sigma(l)\equiv\Sigma(l)-\Sigma_\infty$, respectively, where the subscript ∞ refers to a *free* interface between the adsorbed phase and the middle phase. From this definition we note that the position-dependent contributions $\Delta\kappa(l)$ and $\Delta\Sigma(l)$ vanish in the limit $l\to\infty$.

To enable progress it is convenient to employ a piecewise parabolic (or triple parabola) model and approximate the GL bulk free-energy density by three parabolas [1]. While this

approach facilitates quantitative computations, it is noted that similar results are also anticipated from a ϕ^6 model [24]. For complex fluids one identifies *two* length scales, β_1^{-1} and β_2^{-1} say, which control the domain size of coherent oil and water regions, and the exponential tails in the order-parameter profile. Within this model the bare binding potential is found to take the general form [9,25]

$$W(l)=\sum_{\substack{(i+j>0)\\ i,j=0}}^{\infty}(w_{ij0}-w_{ij1}l)\exp[-(i\beta_1+j\beta_2)l], \tag{2.2}$$

where we assume that $W(l)\to 0$ in the limit of $l\to\infty$. For fixed bulk parameters, which is relevant for our study of unbinding, the values of β_1 and β_2 are fixed and, to allow discussion relating to earlier results [8,9], we assume that $\beta_2<\beta_1<2\beta_2<\beta_2+\beta_1<\cdots$, without loss of generality. Similar expansions are found for the l-dependent parts of the stiffness and rigidity coefficients, i.e.,

$$\Delta\Sigma(l)=\sum_{\substack{(i+j>0)\\ i,j=0}}^{\infty}(s_{ij0}-s_{ij1}l)\exp[-(i\beta_1+j\beta_2)l] \tag{2.3}$$

and

$$\Delta\kappa(l)=\sum_{\substack{i,j=0\\ (i+j>0)}}^{\infty}(k_{ij0}-k_{ij1}l)\exp[-(i\beta_1+j\beta_2)l]. \tag{2.4}$$

To explore the generic behavior of the set of coefficients appearing in these expansions, we introduce the parameter τ to denote the distance (in the space of surface parameters) from the unbinding transition such that $\tau<0$ corresponds to a bound state and $\tau>0$ to an unbound one. With this definition in mind, the mean-field critical transition is controlled by $\tau\to 0^-$. The leading order results for the potential in the triple parabola approximation can then be written as [9,25]

$$w_{010}\approx w_1\tau,\qquad w_{100}\approx -w_2\tau,$$
$$w_{ij1}=0(\forall i,j),\qquad w_{020}\approx w_3, \tag{2.5}$$

where all w_i are positive parameters that may be assumed constant in the vicinity of the transition.

Similarly, the parabolic approximation yields

$$s_{010}\approx s_1\tau,\qquad s_{011}\approx s_2\tau,$$
$$s_{100}\approx -s_3\tau,\qquad s_{101}\approx s_4\tau, \tag{2.6}$$
$$s_{020}\approx s_5,\qquad s_{021}\approx s_6,$$

for the stiffness coefficient [9,25], with strictly positive parameters s_i. We note that the first coefficient in the set of s_{ij1} is nonzero, we will show below that this can have dramatic consequences for the unbinding transitions.

The calculation of the coefficients k_{ij0} and k_{ij1} is nontrivial, even in the triple parabola approximation. Nevertheless, it is straightforward to find a zeroth-order approximation, leading to the following coefficients [9,25]

$$k_{010}\approx k_1\tau,\qquad k_{011}=k_2\tau,$$
$$k_{100}\approx -k_3\tau,\qquad k_{101}=k_4\tau, \tag{2.7}$$
$$k_{020}\approx k_5,\qquad k_{021}\approx k_6,$$

with all $k_i\geqslant 0$.

B. Renormalization group equations

Our task is now to implement a functional RG treatment of the interface Hamiltonian (2.1), an outline of which was introduced in [9]. Here, we present a more detailed analysis and discuss the linear RG flow equations.

Following others [19,21], we write our Hamiltonian in the form $\mathcal{H}_l[l]=\mathcal{H}_0[l]+\mathcal{H}_W[l]$ where $\mathcal{H}_0[l]$ is the free part

$$\mathcal{H}_0[l]=\int d\mathbf{y}\{\tfrac{1}{2}\kappa_\infty(\nabla^2 l)^2+\tfrac{1}{2}\Sigma_\infty(\nabla l)^2\}, \tag{2.8}$$

and $\mathcal{H}_W[l]$ the interaction or wetting part

$$\mathcal{H}_W[l]=\int d\mathbf{y}\{\tfrac{1}{2}\Delta\kappa(l)(\nabla^2 l)^2+\tfrac{1}{2}\Delta\Sigma(l)(\nabla l)^2+W(l)\}. \tag{2.9}$$

Implicitly contained within these definitions is a small-scale cutoff Λ^{-1} (or equivalently a momentum cutoff Λ).

The construction of the functional RG has been well explained elsewhere [18–21,26,27] and so we restrict ourselves to a brief summary of the pertinent points here. The fluctuating field is divided into two parts $l(\mathbf{y})=l^<(\mathbf{y})+l^>(\mathbf{y})$, where $l^<$ represent the small-wave-number or large-scale fluctuations and $l^>$ the large-wave-number or small-scale fluctuations. Hence $l^<$ contains all Fourier components of l with wave numbers in the range $0<|\mathbf{k}|<\Lambda/b$ and $l^>$ those with $\Lambda/b<|\mathbf{k}|<\Lambda$, where $b=e^t$ is the spatial rescaling factor (see below). The fluctuations $l^>$ are integrated out resulting in an effective Hamiltonian, $\mathcal{H}_l'[l^<]$, for the large-scale fluctuations alone. This intermediate, unrescaled, renormalized Hamiltonian is defined via the partial trace

$$\exp\{-\beta\mathcal{H}_l'[l^<]\}=\frac{1}{N}\int\mathcal{D}l^>\exp\{-\beta\mathcal{H}_l[l^<+l^>]\}, \tag{2.10}$$

with $\beta=1/(k_BT)$, and where N is an appropriately defined normalization factor. The crucial assumption of the linear RG is that the perturbation $\mathcal{H}_W$ is small such that it is adequate, when taking the partial trace in Eq. (2.10), to expand in $\mathcal{H}_W$ and retain only the first-order term yielding

$$\mathcal{H}_l'[l^<]=\mathcal{H}_0[l^<]+\mathcal{R}\{\mathcal{H}_W[l^<+l^>]\}, \tag{2.11}$$

where $\mathcal{R}=N^{-1}\int\mathcal{D}l^>\exp\{-\beta\mathcal{H}_0[l^>]\}$ is a linear operator normalized by $\mathcal{R}\{1\}=1$. To evaluate this term we employ

the techniques of Jin and Fisher [21] developed specifically for the situation where a spatially varying stiffness coefficient is present. The idea is to expand $\mathcal{H}_W$ to quadratic order in $l^>$, set $b=e^{\delta t}$ and consider $\delta t \to 0$ so as to derive differential flow equations.

Finally, we must rescale to bring the momentum cut-off back to its original value. In particular it is appropriate to apply the rescaling [26,27]

$$\mathbf{y} \to \mathbf{y}' = \mathbf{y}/b, \quad l(\mathbf{y}) \to l'(\mathbf{y}') = l(\mathbf{y})/b^{\zeta}, \tag{2.12}$$

where $\zeta=(3-d)/2$. It is then straightforward to obtain the set of RG flow equations. First, for the bulk part of the rigidity we find

$$\frac{d\kappa_{\infty}^{(t)}}{dt} = -2\kappa_{\infty}^{(t)}, \tag{2.13}$$

which yields $\kappa_{\infty}^{(t)}=e^{-2t}\kappa_{\infty}$, demonstrating that κ_{∞} simply flows to zero under renormalization. Second, the position-dependent parts of the gradient coefficients, i.e., $\Delta\Sigma(l)$ and $\Delta\kappa(l)$, evolve according to the following equations

$$\frac{\partial \Delta\Sigma^{(t)}(l)}{\partial t} = \zeta l \frac{\partial \Delta\Sigma^{(t)}(l)}{\partial l} + \frac{\Omega}{\Sigma_{\infty}+\kappa_{\infty}\Lambda^2 e^{-2t}} \frac{\partial^2 \Delta\Sigma^{(t)}(l)}{\partial l^2}, \tag{2.14}$$

and

$$\frac{\partial \Delta\kappa^{(t)}(l)}{\partial t} = -2\Delta\kappa^{(t)}(l) + \zeta l \frac{\partial \Delta\kappa^{(t)}(l)}{\partial l} + \frac{\Omega}{\Sigma_{\infty}+\kappa_{\infty}\Lambda^2 e^{-2t}} \frac{\partial^2 \Delta\kappa^{(t)}(l)}{\partial l^2}, \tag{2.15}$$

where, for brevity, we have introduced

$$\Omega = \frac{k_B T \Lambda^{(d-3)}}{(4\pi)^{(d-1)/2}\Gamma\left[\frac{1}{2}(d-1)\right]}. \tag{2.16}$$

In contrast to the above, the flow equation for the interface potential depends explicitly on the other renormalized quantities, with

$$\frac{\partial W^{(t)}}{\partial t} = (d-1)W^{(t)} + \zeta l \frac{\partial W^{(t)}}{\partial l} + \frac{\Omega}{\Sigma_{\infty}+\kappa_{\infty}\Lambda^2 e^{-2t}} \times \left[\frac{\partial^2 W^{(t)}}{\partial l^2} + \Lambda^2 \Delta\Sigma^{(t)} + \Lambda^4 \Delta\kappa^{(t)} \right]. \tag{2.17}$$

The solutions of these flow equations can most easily be found by decoupling the flow of $W^{(t)}$ from that of $\Delta\Sigma^{(t)}$ and $\Delta\kappa^{(t)}$. The details of this procedure for general dimensions d are given in the Appendix, here we only quote the closed-form solutions in $d=3$. From Eqs. (2.14) and (2.15), it is evident that both $\Delta\Sigma^{(t)}$ and $\Delta\kappa^{(t)}$ will evolve in a purely diffusive way, with explicit solutions

$$\Delta\Sigma^{(t)}(l) = \frac{1}{\sqrt{2\pi}g(t)} \int_{-\infty}^{\infty} dl' \Delta\Sigma^{(0)}(l') \times \exp[-(l-l')^2/2g^2(t)], \tag{2.18}$$

and

$$\Delta\kappa^{(t)}(l) = \frac{1}{\sqrt{2\pi}g(t)} \int_{-\infty}^{\infty} dl' \Delta\kappa^{(0)}(l') \times \exp[-(l-l')^2/2g^2(t)], \tag{2.19}$$

where the width of the Gaussian convolution is given by

$$g^2(t) = \frac{k_B T}{4\pi\Sigma_{\infty}} \ln\left(\frac{\Sigma_{\infty} e^{2t} + \kappa_{\infty}\Lambda^2}{\Sigma_{\infty}+\kappa_{\infty}\Lambda^2} \right). \tag{2.20}$$

Furthermore, one finds that the solution for $W^{(t)}$ is of a similar form, with

$$W^{(t)}(l) = \frac{e^{2t}}{\sqrt{2\pi}g(t)} \int_{-\infty}^{\infty} dl' \tilde{W}^{(0)}(l') \exp[-(l-l')^2/2g^2(t)], \tag{2.21}$$

which means that $W^{(t)}$ renormalizes precisely as in the case of constant gradient coefficients [9,19], except that the initial bare potential $W^{(0)}(l)$ is replaced by the modified expression

$$\tilde{W}^{(0)}(l) = W^{(0)}(l) + \frac{k_B T}{8\pi\kappa_{\infty}} f_t \Delta\Sigma^{(0)}(l) + \frac{k_B T \Lambda^2}{8\pi\kappa_{\infty}} \left[1 - e^{-2t} - \frac{\Sigma_{\infty}}{\kappa_{\infty}\Lambda^2} f_t \right] \Delta\kappa^{(0)}(l), \tag{2.22}$$

where f_t is given by

$$f_t = \ln\left(\frac{\Sigma_{\infty}+\kappa_{\infty}\Lambda^2}{\Sigma_{\infty}+\kappa_{\infty}\Lambda^2 e^{-2t}} \right). \tag{2.23}$$

For the study of critical wetting t is large and thus, $\tilde{W}^{(0)}$ essentially differs from $W^{(0)}$ only by fixed terms proportional to $\Delta\Sigma^{(0)}$ and $\Delta\kappa^{(0)}$. Hence at a simple level the effect of the position-dependent gradient coefficients can be gauged from this modified bare potential (see Sec. III). Furthermore, it is apparent from Eq. (2.22) that terms in $\Delta\Sigma^{(0)}$ and $\Delta\kappa^{(0)}$ [see Eqs. (2.3) and (2.4)] can compete with terms in $W^{(0)}$ [Eq. (2.2)] and hence strongly influence the critical behavior. This resembles the situation in simple fluids where it leads to a mechanism destabilizing the critical transition [15,20,21].

III. MEAN-FIELD ANALYSIS OF MODIFIED BARE POTENTIAL FOR CRITICAL UNBINDING

Before we explicitly calculate the renormalized potential by performing the convolution in Eq. (2.21), we first analyze, at a mean-field level, the modified bare potential $\tilde{W}^{(0)}(l)$ given in Eq. (2.22). This will give us a good estimate of the

effect of fluctuations on the bare critical transition.

To begin, it is clear from the above results that this modified potential can be written in the form

$$\tilde{W}^{(0)}(l)=\sum_{\substack{i,j=0\\(i+j>0)}}^{\infty}(\tilde{w}_{ij0}^{(t)}-\tilde{w}_{ij1}^{(t)}l)\exp[-(i\beta_1+j\beta_2)l], \tag{3.1}$$

where the modified coefficients are

$$\tilde{w}_{ijm}^{(t)}=w_{ijm}+\frac{k_BT}{8\pi\kappa_\infty}f_t s_{ijm}+\frac{k_BT\Lambda^2}{8\pi\kappa_\infty}\left(1-e^{-2t}-\frac{\Sigma_\infty}{\kappa_\infty\Lambda^2}f_t\right)k_{ijm}, \tag{3.2}$$

for $m=0,1$. In comparison with the initial bare potential, the most notable feature of Eq. (3.1) is the presence of nonzero terms varying as $l\exp[-(i\beta_1+j\beta_2)l]$, highly analogous to the discoveries for simple fluids [15,20,21]. However, in the present situation, the first of these terms, $-\tilde{w}_{011}^{(t)}le^{-\beta_2 l}$, becomes the *leading-order* contribution in the modified potential, and, unsurprisingly, this drastically alters the predictions for the critical behavior.

In what follows we will frequently drop the terms containing e^{-2t} in the above expressions since they vanish rapidly when t becomes large (as is the case in the regime of interest). Near critical wetting, we can combine the results (2.5)–(2.7) and write

$$\begin{aligned}\tilde{w}_{010}&=\tilde{\tau}\equiv\tau(w_1+c_1s_1+c_2k_1),\\ \tilde{w}_{011}&=\tilde{\tau}q_1\equiv\tau(c_1s_2+c_2k_2),\\ \tilde{w}_{100}&=-\tilde{\tau}p\equiv-\tau(w_2+c_1s_3+c_2k_3),\\ \tilde{w}_{101}&=\tilde{\tau}q_2\equiv\tau(c_1s_4+c_2k_4),\\ \tilde{w}_{020}&=r\equiv w_3+c_1s_5+c_2k_5>0,\\ \tilde{w}_{021}&=q_3\equiv c_1s_6+c_2k_6>0,\end{aligned} \tag{3.3}$$

etc., where c_i, q_i, p, r are positive constants. Note that the first four coefficients are proportional to τ and hence vanish on approach to the mean-field critical phase boundary. Thus, after a rescaling of the thickness l, the modified bare potential reads

$$\tilde{W}^{(0)}(l)=\tilde{\tau}(1-q_1l)e^{-l}-\tilde{\tau}(p+q_2l)e^{-\beta_1 l/\beta_2}+(r-q_3l)e^{-2l}, \tag{3.4}$$

which clearly demonstrates the presence of the new leading order term with coefficient q_1, which, crucially, has the opposite sign to the original leading order term. In the analysis that follows we will typically ignore the second exponential term in Eq. (3.4). This is partly based on explicit evaluation of the various terms within the triple parabola model, which suggests that the coefficients p and q_2 are several orders of magnitude smaller than their counterparts in the first term. Furthermore, an extensive numerical study indicates that this term has no qualitative effect on the phase diagram. We can further estimate the quantitative effect by noting that for $1<\epsilon<2$ we can crudely approximate $e^{-\epsilon l}$ by the interpolated formula $e^{-\epsilon l}\approx(2-\epsilon)e^{-l}+(\epsilon-1)e^{-2l}$. Thus upon setting $\epsilon=\beta_1/\beta_2$ we identify that the main effect of this term is a ''renormalization'' of the other parameters (q_1, r, etc.) with, for example, $q_1\to q_1+(2-\beta_1/\beta_2)q_2$ and $q_3\to q_3+\tau(\beta_1/\beta_2-1)q_2$. Hence we anticipate that the only effect of the second exponential term is to slightly shift the phase boundaries predicted below.

Therefore, to obtain the general phase behavior it suffices to minimize the potential

$$\tilde{W}^{(0)}(l)=\tilde{\tau}(1-q_1l)e^{-l}+(r-q_3l)e^{-2l}, \tag{3.5}$$

and inspect the location of the global minimum as a function of $\tilde{\tau}$, q_1 and q_3. Recall, $\tilde{\tau}$ measures the deviation from the bare critical transition, i.e., the transition determined by the potential $W^{(0)}(l)$. We further set $r=1$ without loss of generality and, although our main interest is for the case of positive q_1 and q_3, we do consider both positive and negative values of these parameters in order to take into account a possible shift due to q_2 (see above). For clarity we consider slices through the phase diagram with fixed q_3 or fixed q_1, and collect our results together at the end of this section.

A. $(\tilde{\tau},q_1)$ diagrams for fixed q_3

We start with a comprehensive study of the potential for fixed q_3. The most notable feature is that for positive q_1, the leading-order term will change sign as compared to the original potential. Clearly, this will have a dramatic effect on the phase behavior, and in Fig. 2 we present some typical examples of phase diagrams showing q_3 fixed zero, negative, and positive. Further details are provided below.

Let us first consider the simplest case when $q_3=0$ [Fig. 2(a)], for which the analysis is relatively straightforward. We distinguish four regions, separated by first-order or continuous phase boundaries. When $\tilde{\tau}$ and q_1 are both positive, $\tilde{W}^{(0)}(l)$ has a minimum at finite l corresponding to a bound (B) state. As $q_1\to0$, however, the location of this minimum diverges according to

$$l\approx\frac{1}{q_1}, \tag{3.6}$$

such that there is a critical unbinding transition for $q_1=0$, $\tilde{\tau}>0$ (dotted line). Indeed, in the upper left corner of the diagram, all terms in the potential are positive and the interface will be unbound (UB). In addition, when taking $\tilde{\tau}\to0^+$ while keeping q_1 strictly positive, the thickness also continuously diverges with

$$l\approx\ln\left(\frac{1}{|\tilde{\tau}|}\right), \tag{3.7}$$

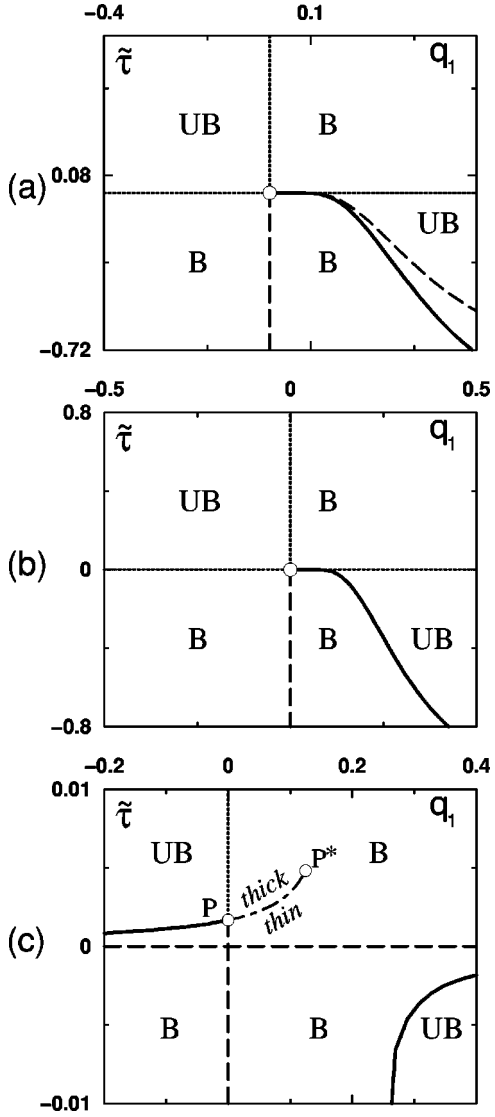

FIG. 2. $(\tilde{\tau},q_1)$ mean-field phase diagrams for (a) $q_3=0$, (b) $q_3=-0.25$, and (c) $q_3=0.25$, showing unbound (UB) and bound (*B*) regions. The phase boundaries are shown by dotted (critical) and solid (first-order) lines, while the dashed lines denote metastable limits. The open circle in (a) and (b) represents a multicritical point. Further, the dashed-dotted line in (c) marks a thin-thick transition, with *P* and *P** both being critical end points.

and hence another critical boundary is identified. Similarly when $\tilde{\tau}$ and q_1 are both negative, the interface is also bound with a continuous transition for $\tilde{\tau}\to 0^-$ and where the interface again diverges according to Eq. (3.7). Hence the dotted line $\tilde{\tau}=0$ represents a continuous phase boundary for all q_1.

In the final quadrant of the diagram the interplay between positive and negative contributions to $\tilde{W}^{(0)}(l)$ suggests the possibility of a first-order transition. By minimizing the potential in this regime, we indeed find a first-order unbinding transition represented in Fig. 2(a) by the solid line. The thickness l_0 of the adsorbed layer at the point of the transition, i.e., prior to the jump to infinity, is given by $l_0=1/q_1-1$, and the transition boundary reads

$$\tilde{\tau}_0=-\frac{1}{q_1}e^{(q_1-1)/q_1}. \tag{3.8}$$

We further can identify the two metastable limits connected to the first-order transition, these are shown by the dashed lines. By considering just the tail of the potential it is clear that the line $q_1=0$ marks the point where the extremum at $l=\infty$ changes its character from being a local minimum to a local maximum, and hence corresponds to the metastable limit for the unbound state. For the other metastable limit we find

$$\tilde{\tau}_{\mathrm{ML}}=-\frac{2}{q_1}e^{-1/q_1}. \tag{3.9}$$

Within this phase diagram the origin acts as a multicritical point.

For negative q_3, the phase diagram remains qualitatively unchanged, a representative example is given in Fig. 2(b) for $q_3=-0.25$. However, due to the presence of the q_3 term the computation of the first-order boundary is a little more involved and analytic results are more complex, although still attainable. For example, we obtain

$$\tilde{\tau}_0=-\frac{1+q_3-q_3l_0}{q_1}e^{-l_0}, \tag{3.10}$$

where $l_0=[q_1+q_3-\{(q_1-q_3)(q_1-q_3+4q_1q_3)\}^{1/2}]/2q_1q_3$ again represents the thickness at the transition point. We refrain from calculating the metastable limit of the bound state in this case, although numerical studies suggest it is likely to be of the same form as Eq. (3.10) for small q_1.

It is much more interesting to discuss the change in the diagram as q_3 becomes positive. As demonstrated in Fig. 2(c) for $q_3=0.25$, a very different situation is found, including some extra transitions. We start by noting that the critical transition found in the previous cases when $\tau\to 0^-$ for $q_1<0$ is lost, but is replaced by a first-order transition at positive, small τ values (note the enlarged scale). This transition line terminates at a *critical end point P* with coordinates

$$q_1=0, \quad \tilde{\tau}=q_3\exp[-(1+q_3)/q_3]. \tag{3.11}$$

Note that in this case there is only one critical phase boundary and that the origin is no longer a multicritical point. Beyond *P* into the bound region, we further find a *thin-thick* transition boundary (dashed-dotted line) which, in turn, extends from *P* to a second critical end point *P** with coordinates

$$q_1=\frac{q_3}{1+4q_3}, \quad \tilde{\tau}=(1+4q_3)\exp[-(1+2q_3)/q_3], \tag{3.12}$$

where the two thicknesses, l_1 and l_2 say, become identical. Finally, another first-order unbinding transition is found in the bottom right corner of the figure (where $\tilde{\tau}<0$ and $q_1>0$). Although not apparent on the scale shown, this phase boundary bends back to larger values of q_1 for large, nega-

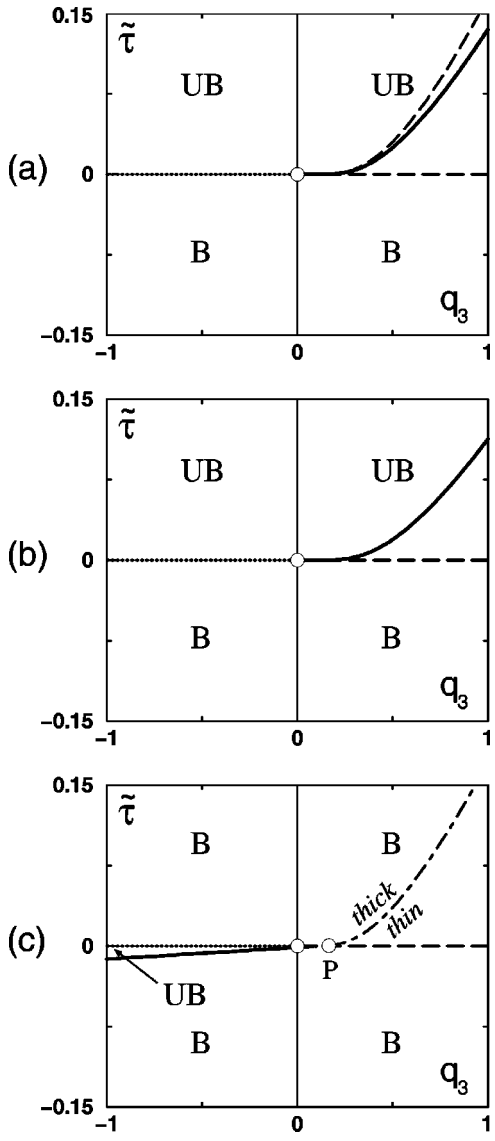

FIG. 3. $(\tilde{\tau},q_3)$ mean-field phase diagrams for (a) $q_1=0$, (b) $q_1=-0.1$, and (c) $q_1=0.1$, showing unbound (UB) and bound (*B*) regions. The phase boundaries are shown by dotted (critical) and solid (first-order) lines, while the dashed lines denote metastable limits. In each case, the origin is a tricritical point. In (c), the thin-thick transition line, originating at the point *P*, is given by the dashed-dotted line.

tive $\tilde{\tau}$ (as will be clarified at the end of this section) yielding the possibility of *reentrant* behavior. As before, the dashed lines correspond to the metastable limits for the unbound state.

B. $(\tilde{\tau},q_3)$ diagrams for fixed q_1

To gain a complete insight into the phase behavior prescribed by the potential $\tilde{W}^{(0)}(l)$, it is instructive to repeat the above analysis for fixed q_1 and to briefly comment on typical $(\tilde{\tau},q_3)$ diagrams.

The case $q_1=0$, shown in Fig. 3(a), is directly analogous to the situation for simple fluids with a position-dependent stiffness coefficient, as studied by Fisher and Jin [15] and Jin and Fisher [20,21]. For negative q_3 the bare mean-field predictions are not affected by the stiffness term resulting in a critical transition when $\tau\to 0^-$ with a divergence given by Eq. (3.7). When $q_3>0$, on the other hand, fluctuation-induced first-order behavior is observed. The transition boundary can easily be computed and reads

$$\tilde{\tau}_0=q_3 e^{-(q_3+1)/q_3}, \tag{3.13}$$

with the thickness at the transition point given by $l_0=1/q_3+1$. Note again the exponential behavior in Eq. (3.13) and that the origin is a tricritical point. As before, the first-order transition is accompanied by two metastable limits, one of which is given by $\tilde{\tau}=0$, whereas the other is

$$\tilde{\tau}_{\mathrm{ML}}=2q_3\exp[-(3q_3+2)/2q_3]. \tag{3.14}$$

The inclusion of a negative q_1 value does not essentially alter the physics, hence the resulting phase diagram [see Fig. 3(b)] strongly resembles the previous one, with only small quantitative modifications.

On the other hand, for positive q_1, we predict significant changes in the diagram, as exemplified in Fig. 3(c). The most striking feature is that for $\tilde{\tau}>0$ the interface is now always bound, which results from the change in sign of the leading order term in the potential. The first-order unbinding transition seen in the previous two cases ceases to exist and is replaced by a thin-thick transition (dashed-dotted line). This boundary does not originate at the origin but at the point *P* with coordinates

$$q_3=\frac{q_1}{1-4q_1}, \quad \tilde{\tau}=0, \tag{3.15}$$

when $q_1<0.25$. For $q_1\geqslant 0.25$ there is no longer a thin-thick transition within the phase space.

We find a small unbound region in the phase diagram that gives rise to reentrant behavior. In particular, if we decrease $\tilde{\tau}$ from a positive value (with $q_3<0$) we find that the thickness of the adsorbed layer continuously diverges as $\tilde{\tau}\to 0^+$ [with l again given by Eq. (3.7)], therefore the dotted line represents a critical unbinding transition. By further lowering $\tilde{\tau}$ we return to a bound state via a first-order transition (solid line). Albeit hardly visible in the figure, the reentrant behavior is also observed for slightly positive q_3, with the borders of the unbound region in this case given by two first-order transitions (so that the origin remains a tricritical point). Specifically, we find that this occurs in the range $0<q_3<q_1$.

This behavior is more clearly seen in a three-dimensional phase diagram plotted in the variables $\tilde{\tau}$, q_1, and q_3 that summarizes our results of this section. This is shown schematically in Fig. 4 where, for convenience, we restrict ourselves to the unbinding transitions without indicating the thin-thick transition surfaces. It is apparent from this figure that for q_1 and q_3 positive (which is the relevant case) varying $\tilde{\tau}$ from a negative value to a positive one either yields no phase transition with the interface always bound, or gives

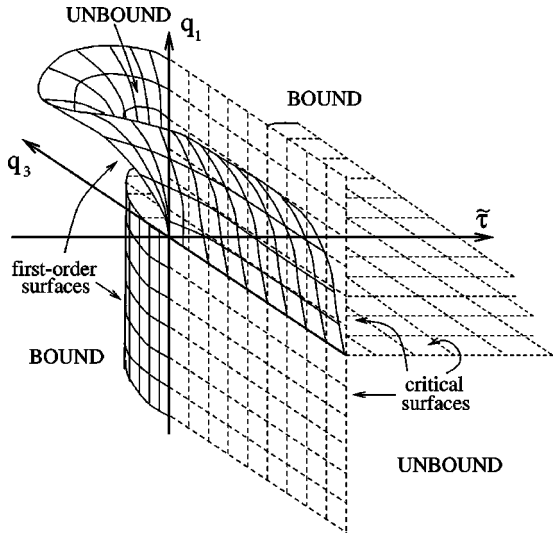

FIG. 4. Schematic three-dimensional surface phase diagram in the variables $\tilde{\tau}$, q_1, and q_3. The critical and first-order unbinding transition surfaces are indicated by dashed and solid lines, respectively.

two consecutive first-order transitions from bound to unbound, and back to bound again. Thus our mean-field analysis of the modified bare potential indicates that the bare critical unbinding transition is lost under renormalization and in this region of the phase diagram it is difficult (or impossible) for the interface to become unbound. We expect the analysis of this section to be a good guide to the renormalized behavior provided the fluctuation effects are weak [19,21]; motivated by this study we now return to the functional RG to investigate the full range of fluctuation behavior.

IV. RENORMALIZATION-GROUP RESULTS FOR CRITICAL UNBINDING

A rigorous application of the RG for the bare critical wetting transition essentially involves performing the convolution in Eq. (2.21), which is the issue we now address. In order to investigate unbinding phenomena using the RG we must implement a matching procedure since, as noted by Fisher and Huse, there is no nontrivial fixed point representing the unbinding transition [19]. In particular we renormalize up to a scale $t^\dagger$ at which the curvature of the renormalized potential at the minimum is of order one, at this point one may expand the potential around the minimum and use mean-field theory to estimate the correlation length $\xi_\parallel$. Thus one finds the location of the minimum, $l^\dagger$ say, and $t^\dagger$ from the requirements

$$\left.\frac{\partial W^{(t)}(l)}{\partial l}\right|_{l^\dagger}=0, \tag{4.1}$$

and

$$\left.\frac{\partial^2 W^{(t^\dagger)}}{\partial l^2}\right|_{l^\dagger}\approx\Sigma_\infty, \tag{4.2}$$

where Σ_∞ is assumed positive. At this scale the correlation length parallel to the interface, $\xi_\parallel$, will also be of order one and hence from Eq. (2.12) the original parallel correlation length is $\xi_\parallel\approx e^{t^\dagger}$. At critical unbinding this correlation length diverges, so $t^\dagger\to\infty$. Further, applying mean-field theory at the matching point yields a renormalized interfacial thickness $l^\dagger$ and since there is no rescaling of perpendicular distances in $d=3$ [see Eq. (2.12)], we obtain the original layer thickness $\langle l\rangle=l^\dagger$.

The convolution (2.21) for the potential is defined over the range $-\infty<l<\infty$, whereas our expressions for $\tilde{W}^{(0)}(l)$ have only been given thus far for $l\geqslant 0$. In practice the unbinding fluid interface cannot pass through the wall at $z=0$ so one should formally include a hard-wall restriction such that W is infinite for $l<0$. However, the linearized RG cannot properly handle a potential that diverges to infinity; so, instead, we settle for the soft-wall restriction $W^{(0)}(l)=c>0$ for $l<0$. Monte Carlo simulations of a lattice version of the interface model suggest that this approximation has no significant effect on the results, with both hard- and soft-wall restrictions yielding the same critical behavior [28].

We must further assign values for $\Delta\Sigma^{(0)}(l)$ and $\Delta\kappa^{(0)}(l)$ for $l<0$. Here we follow the lead of Jin and Fisher and adopt the choice $\Delta\Sigma^{(0)}(l)=\Delta\kappa^{(0)}(l)=0$ for $l<0$. This means that the interface has fixed stiffness and rigidity contributions, Σ_∞ and κ_∞, respectively, for $l<0$ but varies in the way described by Eqs. (2.3) and (2.4) for positive l. Alternative choices are possible but will typically be equivalent to small modifications to the soft wall contribution c for the binding potential [21], hence we do not pursue these any further here.

At this point the renormalized potential can be obtained quite straightforwardly by solving the integral in Eq. (2.21) by the method of steepest descent. To analyze the different regimes it is very convenient to divide the modified bare potential $\tilde{W}^{(0)}(l)$ into its constituent parts

$$\tilde{W}^{(0)}(l)=W_c(l)+W_{q_1}(l)+W_{q_3}(l), \tag{4.3}$$

where we define

$$W_c^{(0)}(l)=\begin{cases} c, & l<0 \\ 0, & l>0, \end{cases} \tag{4.4}$$

$$W_{q_1}^{(0)}(l)=\begin{cases} \tilde{\tau}(1-q_1 l)e^{-l}, & l>0 \\ 0, & l<0, \end{cases} \tag{4.5}$$

and

$$W_{q_3}^{(0)}(l)=\begin{cases} (1-q_3 l)e^{-2l}, & l>0 \\ 0, & l<0. \end{cases} \tag{4.6}$$

We further note that when t is large, as is relevant for studying critical unbinding, the width of the convolution, $g^2(t)$, behaves as $g^2(t)\approx 2\omega t$. Here ω is the capillary parameter given by $\omega=k_BT/(4\pi\Sigma_\infty\xi_b^2)$, with $\xi_b=\beta_2^{-1}$ the bulk correlation length of the adsorbed phase.

We first consider the renormalization of $W_{q_1}(l)$, which can be written explicitly as

$$W^{(t)}_{q_1}(l)=\frac{e^{2t}\tilde{\tau}}{\sqrt{4\pi\omega t}}\int_0^\infty dl'(1-q_1 l')\exp[-l'-(l'-l)^2/4\omega t]. \tag{4.7}$$

The exponent in this integral is maximized at $l'_s=l-2\omega t$, so that for $l>2\omega t$ the integral is dominated by the saddle point at l'_s, yielding

$$W^{(t)}_{q_1}(l)\approx\tilde{\tau}[1-q_1(l-2\omega t)]e^{(2+\omega)t-l}. \tag{4.8}$$

Conversely, when $l<2\omega t$ the integral in Eq. (4.7) will be dominated by its contribution near zero that gives

$$W^{(t)}_{q_1}(l)\approx\frac{1}{\sqrt{4\pi\omega t}}\frac{\tilde{\tau}}{1-l/2\omega t}\left[1-\frac{q_1}{1-l/2\omega t}\right]e^{2t-l^2/4\omega t}. \tag{4.9}$$

We thus see that the renormalized $W_{q_1}(l)$ decays exponentially for $l>2\omega t$, while for $l<2\omega t$ it is a Gaussian. Arguing along the same lines, we find that

$$W^{(t)}_{q_3}(l)\approx[1-q_3(l-4\omega t)]e^{(2+4\omega)t-2l}, \tag{4.10}$$

for $l>4\omega t$, while for $l<4\omega t$

$$W^{(t)}_{q_3}(l)\approx\frac{1}{\sqrt{4\pi\omega t}}\frac{1}{2-l/2\omega t}\left[1-\frac{q_3}{2-l/2\omega t}\right]e^{2t-l^2/4\omega t}. \tag{4.11}$$

Lastly, renormalizing the wall-part of the potential, we find

$$W^{(t)}_{c}(l)\approx\frac{c}{\sqrt{4\pi\omega t}}\frac{2\omega t}{l}e^{2t-l^2/4\omega t} \tag{4.12}$$

for all $l>0$. To elucidate the renormalized transition behavior we now analyze the various fluctuation regimes distinguished by the value of the capillary parameter ω.

A. Regime I: Weak fluctuations

We begin by considering the case $l>4\omega t$. It is clear by inspection that in this case $W^{(t)}_c(l)$ is a higher-order contribution and so at leading orders we have

$$W^{(t)}(l)\approx\tilde{\tau}[1-q_1(l-2\omega t)]e^{(2+\omega)t-l}+[1-q_3(l-4\omega t)]e^{(2+4\omega)t-2l}. \tag{4.13}$$

We initially concentrate on obtaining the renormalized phase diagram for the situation when $q_3=0$. Upon using the matching technique we obtain from Eq. (4.1) and (4.2)

$$\tilde{\tau}\approx\left[\frac{-2}{1-q_1(l^\dagger-2\omega t^\dagger-1)}\right]e^{3\omega t^\dagger-l^\dagger}, \tag{4.14}$$

$$\Sigma_\infty\approx 2\left[\frac{1-q_1(l^\dagger-2\omega t^\dagger)}{1-q_1(l^\dagger-2\omega t^\dagger-1)}\right]\exp[(2+4\omega)t^\dagger-2l^\dagger], \tag{4.15}$$

from which we can determine $l^\dagger$ and $t^\dagger$. Doing so we find that the ansatz $l>4\omega t$ is justified only for $\omega<\frac{1}{2}$ (which we denote as regime I), just as in the case of earlier RG studies [19,21]. We further define the renormalized singular part of the potential $F_s=e^{-2t^\dagger}W^{(t^\dagger)}(l^\dagger)$, which in this regime can be written as

$$F_s=-[1+q_1\tilde{\tau}e^{-3\omega t^\dagger+l^\dagger}]e^{4\omega t^\dagger-2l^\dagger}. \tag{4.16}$$

From this expression we observe that $F_s\leqslant 0$ when $q_1\tilde{\tau}>0$ (i.e., for $q_1<0,\tilde{\tau}<0$ and for $q_1>0,\tilde{\tau}>0$). In the quadrant $q_1<0,\tilde{\tau}>0$ all terms in Eq. (4.13) are positive (for $q_3=0$) and so the interface is unbound in this region. As a result we distinguish two different critical unbinding transitions, one of which occurs for $|\tilde{\tau}|\to 0$ and the other for $q_1\to 0^+$ and $\tilde{\tau}>0$.

We denote the singularities of the first of these transitions using a superscript *. For example, the thickness $\langle l\rangle^*$ of the wetting layer behaves as

$$\langle l\rangle^*\approx\frac{1+2\omega}{1-2\omega}\left\{\ln\left[\frac{2}{|\tilde{\tau}|}\right]-\ln\left[1+\frac{q_1}{1-\omega}\ln\left[\frac{|\tilde{\tau}|}{2}\right]+\cdots\right]\right\}, \tag{4.17}$$

as $|\tilde{\tau}|\to 0$ and where the dots represent noncritical terms. Note that the presence of q_1 only introduces a subsidiary $\ln\ln|\tilde{\tau}|$ singularity. The result for the parallel correlation length reads

$$\xi^*_\parallel\sim|\tilde{\tau}|^{-1/(1-\omega)}, \tag{4.18}$$

which yields the usual critical exponent $\nu^*_\parallel=1/(1-\omega)$ for regime I [15,19,21].

The singularities found for the other critical transition, i.e., for $q_1\to 0^+$, are fundamentally different. Indeed, even on a mean-field level, we found that the thickness diverged in an algebraic fashion [see Eq. (3.6)] rather than logarithmically, and this is again found in the renormalized behavior. In particular, using a superscript $\times$ to denote singularities associated with this transition, we find for the thickness

$$\langle l\rangle^\times=\frac{2+\omega}{2-\omega}\left(1+\frac{1}{q_1}\right)+\frac{2\omega}{2-\omega}\ln\left[\frac{\Sigma_\infty}{\tilde{\tau}q_1}\right]. \tag{4.19}$$

This behavior has been determined using only the first exponential in Eq. (4.13) that seems reasonable for $\tilde{\tau}>0$. Explicit calculations reveal that including the second exponential in the potential only leads to a small correction to the above result of the form $q_1^{-1}e^{-1/q_1}$. The correlation length for this transition grows *exponentially* fast as described by

$$\xi^\times_\parallel=(\tilde{\tau}q_1)^{-\theta_1}\exp[\theta_1(1+1/q1)], \tag{4.20}$$

where $\theta_1 = 1/(2-\omega)$ and, therefore, $\nu_\parallel^\times = \infty$.

As in the mean-field phase diagram a first-order transition is predicted in the region $q_1 > 0, \tilde{\tau} < 0$ going from bound ($|\tilde{\tau}|$ large) to unbound ($|\tilde{\tau}|$ small). The axis $\tilde{\tau} = 0$ remains a second-order phase boundary with the same critical behavior as predicted when $q_1 < 0$, i.e., Eqs (4.17) and (4.18). We locate the first-order phase boundary by setting $F_s = 0$ in Eq. (4.16), and find that the layer thickness just prior to the transition is given by

$$\langle l \rangle_0 = (1+2\omega)\left(\frac{1-q_1}{q_1}\right) + \omega \ln \Sigma_\infty , \tag{4.21}$$

for small q_1. Likewise, one finds

$$\xi_{\parallel 0} \approx \sqrt{\Sigma_\infty} e^{(1-q_1)/q_1}. \tag{4.22}$$

Using these results we obtain the transition boundary

$$\tilde{\tau}_0 = -\frac{(\Sigma_\infty)^{\omega/2}}{q_1} \exp[-(1-\omega)(1-q_1)/q_1], \tag{4.23}$$

as $q_1 \to 0^+$. We note that all of the above reduce to their mean-field counterparts in the limit $\omega \to 0+$. The $q_3 = 0$ phase diagram, incorporating all of these results, is qualitatively identical to the corresponding mean-field diagram [see Fig. 2(a)].

The above analysis becomes more involved for $q_3 \neq 0$ although analytic progress is possible. In particular, if $q_3 < 0$ the phase diagram remains unchanged with leading order critical behavior identical to the $q_3 = 0$ case described above. For example, the layer thickness $\langle l \rangle^*$ for the transition when $|\tilde{\tau}| \to 0$ is still given by Eq. (4.17) up to corrections of the form $\ln[1 + q_3 \ln(|\tilde{\tau}|^{-1})]$ so that the critical exponents are unchanged. Inspection of Eq. (4.13) reveals that for $q_3 \leqslant 0$ the contribution from the second exponential is always positive and so it is no surprise that the $q_3 = 0$ and $q_3 < 0$ behaviors are qualitatively the same.

For $q_3 > 0$ the situation is more complicated as already suggested by Fig. 2. In this case the additional exponential contribution related to q_3 is a destabilizing factor, in particular when $|\tilde{\tau}|$ is small. In analogy with the earlier study of Fisher-Jin this leads to the critical transitions along the $\tilde{\tau} = 0$ axis being driven fluctuation-induced first-order with the corresponding phase boundaries being shifted to $q_1 \tilde{\tau} < 0$ regions of the phase diagram. For $q_1 < 0$ there is always a first-order phase boundary that terminates at the point P with coordinates

$$q_1 = 0, \quad \tilde{\tau} = \tilde{\tau}_P = \Sigma_\infty \left(\frac{q_3}{\Sigma_\infty}\right)^{\theta_2} \exp[-\theta_3(1 + 1/q_3)], \tag{4.24}$$

where $\theta_2 = [1 - 3/(2\omega)]/(1-2\omega)$ and $\theta_3 = (1-\omega)/(1-2\omega)$. Qualitatively Fig. 2(c) provides an accurate representation of the phase diagram in this regime. This is also true for $q_1 > 0$ for which we identify reentrant behavior for fixed q_1 sufficiently large. Explicit calculations reveal no phase transitions for q_1 in the range $0 < q_1 < f(\omega) q_3$. Here $f(\omega)$ is an unwieldily complicated function of ω that displays surprisingly simple behavior such that $f(\omega) \to 1$ as $\omega \to 0$ and $f(\omega) \gtrsim 1$ for $0 < \omega < 1/2$. For fixed $q_1 > f(\omega) q_3$ we predict a sequence of two first-order transitions (from bound to unbound, and back to bound) as $\tilde{\tau}$ is varied from zero to large negative values.

Finally, as $q_1 \to 0^+$ we still predict a second-order transition provided $\tilde{\tau} > \tilde{\tau}_P$. For this transition it is again essentially only the first exponential term in Eq. (4.13) that is important and so we predict the same critical singularities as found for the $q_3 = 0$ case described above. In particular, the layer thickness $\langle l \rangle^\times$ is given by Eq. (4.19) and $\nu_\parallel^\times = \infty$.

B. Regime II: Intermediate fluctuations

The second regime is given when l is restricted such that $2\omega t < l < 4\omega t$. In this regime, the interface potential is

$$W^{(t)}(l) \approx \tilde{\tau}[1 - q_1(l - 2\omega t)] e^{(2+\omega)t - l} + \frac{K(l/2\omega t)}{\sqrt{t}} e^{2t - l^2/4\omega t}, \tag{4.25}$$

where $\sqrt{4\pi\omega} K(x) = 1/(2-x)[1 - q_3/(2-x)] + c/x$. For $q_3 = 0$ it is sufficient to consider $K(l/2\omega t) \approx K$ constant in order to find the leading order critical behavior. The minimum and curvature matching formulas (4.1) and (4.2) yield

$$-\tilde{\tau}[1 - q_1(l^\dagger - 2\omega t^\dagger - 1)] = \frac{K l^\dagger}{2\omega t^{\dagger 3/2}} \exp[-(l^\dagger - 2\omega t^\dagger)^2/4\omega t^\dagger] \tag{4.26}$$

and

$$\exp[l^\dagger - (2 + \omega t^\dagger)]\Sigma_\infty \approx \tilde{\tau}[1 - q_1(l^\dagger - 2\omega t^\dagger - 2)] + \frac{K}{2\omega t^{\dagger 3/2}}\left[\frac{l^{\dagger 2}}{2\omega t^\dagger} - 1\right] \times \exp[-(l^\dagger - 2\omega t^\dagger)^2/4\omega t^\dagger]. \tag{4.27}$$

Solving these equations for large t reveals that for transitions associated with vanishing $\tilde{\tau}$ one has $l^\dagger \approx \sqrt{8\omega} t^\dagger$, while $q_1 \to 0$ transitions have $l^\dagger \approx (2+\omega) t^\dagger$. This latter behavior is also found in regime I since only the first exponential term is required for determining the critical behavior. Thus the results of regime II are valid whenever $1/2 < \omega < 2$.

Associated with these two limits we again identify two critical transitions. First, when $|\tilde{\tau}| \to 0$, the thickness diverges as

$$\langle l \rangle^* \approx \frac{\sqrt{8\omega}}{(\sqrt{2} - \sqrt{\omega})^2} \ln\left[\frac{1}{|\tilde{\tau}|}\right], \tag{4.28}$$

with leading order corrections of $\mathcal{O}(\ln[\ln(|\tilde{\tau}|)])$. We further find

$$\xi_{\|}^{*} \sim \left\{ |\tilde{\tau}| \left[\ln\left(\frac{1}{|\tilde{\tau}|} \right) \right]^{\sqrt{\omega/8}} \times \left[1 - \frac{2\sqrt{\omega} q_1}{\sqrt{2}-\sqrt{\omega}} \ln\left(\frac{1}{|\tilde{\tau}|} \right) \right]^{\sqrt{\omega/2}} \right\}^{-1/(\sqrt{2}-\sqrt{\omega})^2}, \tag{4.29}$$

and thus $\nu_{\|}^{*} = 1/(\sqrt{2}-\sqrt{\omega})^2$ in agreement with standard critical wetting results for regime II [19]. For the other critical transition $^{\times}$ we recall from above that the dominant singular behavior is determined from the first exponential term in the renormalized potential, and hence the basic results of regime I, i.e., Eqs. (4.19) and (4.20), also apply in the present regime.

In addition to the critical transitions we still have a first-order transition for $q_1 > 0$ and $\tilde{\tau} < 0$ such that the topology of the phase diagram for $q_3 = 0$ is identical to Fig. 2(a). For completeness we note that upon setting $F_s = e^{-2t^{\dagger}} W^{(t^{\dagger})}(l^{\dagger})$ to zero we identify the loci of the first-order phase boundary as

$$\tilde{\tau}_0 \sim -\frac{1}{q_1} \exp[-(\sqrt{2/\omega}-1)/2q_1], \tag{4.30}$$

for small q_1, in this regime.

For $q_3 < 0$ the critical behavior is qualitatively unchanged since, as can be seen from Eq. (4.25), the q_3 contribution is always positive in this regime and can be incorporated into the constant K when determining leading order behavior.

For $q_3 > 0$ the phase behavior is very rich with two different scenarios dependent upon the magnitude of q_3. The crossover occurs when $q_3 = Q_3(\omega)$ where

$$Q_3(\omega) = \sqrt{\frac{2}{\omega}} [1 + (\sqrt{2\omega}-1)c](\sqrt{2\omega}-1), \tag{4.31}$$

and the presence of the wall strength c indicates that results in this regime will depend quantitatively on the treatment of the wall restriction. When $q_3 < Q_3(\omega)$ the negative contribution to the second exponential is insufficient to destabilize the critical unbinding transition at $|\tilde{\tau}| = 0$. Thus the critical transition remains in this case with leading order critical behavior described by Eqs. (4.28) and (4.29). Furthermore, the origin remains a multicritical point with a first-order phase boundary in the lower right quadrant of the phase diagram [see (4.30)] and the second critical transition $^{\times}$ for $q_1 = 0, \tilde{\tau} > 0$. Hence the phase diagram is qualitatively the same as for $q_3 = 0$ as shown schematically in Fig. 5(a).

Conversely, when $q_3 > Q_3(\omega)$ the q_3 contribution destabilizes the * transition with the phase transition being driven first order. For $q_1 \leqslant 0$ the transition boundary is shifted into the positive $\tilde{\tau}$ region of the phase diagram and terminates on the $q_1 = 0$ axis at the point P where

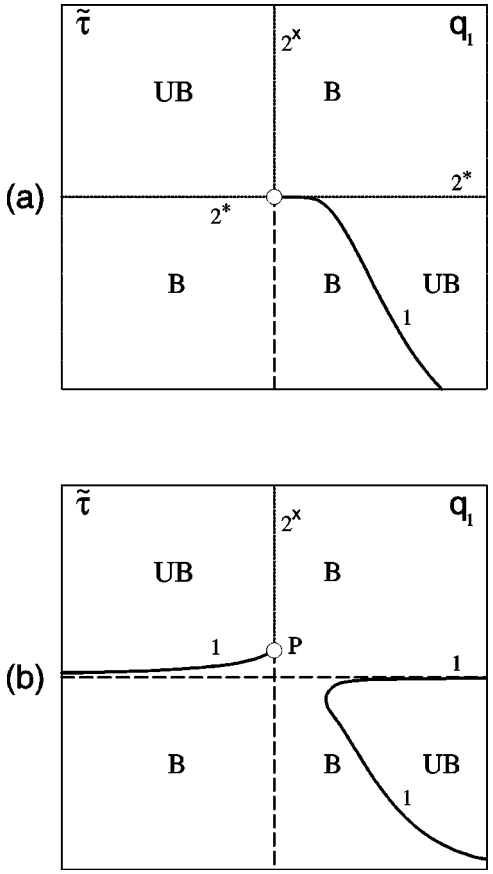

FIG. 5. Schematic renormalized $(\tilde{\tau}, q_1)$ phase diagrams in regime II for the cases (a) $q_3 < Q_3(\omega)$ and (b) $q_3 > Q_3(\omega)$. The loci of critical unbinding transitions are given by the dotted lines, with the superscripts indicating the two essentially different types of transition. Thick lines represent the first-order transition phase boundaries. The dashed lines correspond to the metastability limits of the unbound state, and P identifies the critical end point described in the main text.

$$\tilde{\tau} \sim \exp\left(-\frac{3(\sqrt{2}-\sqrt{\omega})^2}{2\sqrt{8\omega}} \frac{1}{q_3 - Q_3} \ln\left[\frac{1}{q_3 - Q_3} \right] \right). \tag{4.32}$$

For $q_1 > 0$ the phase boundary for the fluctuation-induced first-order unbinding transition smoothly connects with the usual first-order boundary as shown schematically in Fig. 5(b). When $q_1/q_3 \lesssim 1$ there is no unbinding transition for fixed q_1, while for larger fixed q_1 we have reentrant behavior.

C. Regime III: Strong fluctuations

The final fluctuation regime is given for $l < 2\omega t$. In this case all the parts of the renormalized potential take the form of Gaussians with

$$W^{(t)}(l) \approx \frac{\overline{K}(l/2\omega t)}{\sqrt{4\pi\omega t}} e^{2t - l^2/4\omega t}, \tag{4.33}$$

where $\overline{K}(x)=\tilde{\tau}/(1-x)[1-q_1/(1-x)]+1/(2-x)[1-q_3/(2-x)]+c/x$. Identifying $l^\dagger$ and $t^\dagger$ using the matching requirements (4.1) and (4.2) reveals that the ansatz $l<2\omega t$ corresponds to the restriction $\omega>2$ that defines regime III. The best estimates for the capillary parameter suggest $\omega \approx 0.75$ [Refs. [29–31]] and so we do not expect regime III to be relevant for comparison with Monte Carlo simulation studies. Hence we forgo a detailed derivation of the phase diagram in this regime and simply describe the main features.

The overall phase diagram is topologically the same as in regime II although the precise location of the phase boundaries are modified. Once again there is a crossover value $\overline{Q}_3(\omega)$ such that for $q_3<\overline{Q}_3$ the * transition remains critical and for $q_3>\overline{Q}_3$ the transition is fluctuation-induced first order. In the first case the phase boundary is shifted from the $\tilde{\tau}=0$ axis, further the $^\times$ transition phase boundary is also shifted from the $q_1=0$ axis and where the two transition lines meet there is a multicritical point from which a first-order phase boundary emerges. For both of the critical transitions we identify exponential growth for the parallel correlation length so $\nu^*=\nu^\times=\infty$. For $q_3>\overline{Q}_3$ the phase diagram is similar to Fig. 5(b) although the critical transition line is slightly shifted from the $q_1=0$ axis. Crucially there are still two disconnected regions of unbounded phase as shown in the figure.

V. RENORMALIZED SURFACE PHASE DIAGRAM

The RG analysis of the previous sections has demonstrated that fluctuation effects will strongly modify the mean-field predictions for phase behavior with the position dependence of the stiffness and rigidity being of vital importance. In this section we wish to understand how this modified behavior in the space of $\tilde{\tau}$, q_1, and q_3 can be interpreted in terms of the surface parameters, and in particular how a typical mean-field surface phase diagram as exemplified in Fig. 1, will change under renormalization. To do this we must first determine the dependence of q_1 and q_3 upon the surface parameters, most notably the surface field μ_s and enhancement ω_s, in the critical regime. Second, we must consider the issue of renormalization effects upon the bare first-order transition shown in Fig. 1.

To address the first of these issues we note from Eq. (3.3) that q_3/q_1 can be written in terms of the stiffness and rigidity coefficients s_2, s_6, k_2, and k_6. We further observe from explicit calculation within the triple parabola model that in each case the stiffness contribution dominates over the rigidity one such that $q_3/q_1 \approx s_6/s_2$. Both of the contributions s_2 and s_6 are strictly positive near the critical transition. Consequently, only the results of the RG analysis for positive q_1 and q_3 are relevant in determining the renormalization of the critical boundary. We restrict our attention in this section to $\omega<2$ (i.e., regimes I and II) as seems reasonable for comparison with simulations. For these cases we see from the last section that if $q_1 \gtrsim q_3$ we predict reentrant behavior crossing two first-order transition boundaries as $\tilde{\tau}$ is varied. However, when q_1 is significantly smaller than q_3 there is no transition and the interface is always predicted to be bound. Recall $\tilde{\tau}$ is simply a measure of the deviation from the mean-field critical wetting phase boundary so varying $\tilde{\tau}$ explores the vicinity of the mean-field transition boundary in the surface phase diagram. For concreteness we consider a fixed value of $|\mu_s|$ and explore the phase diagram by varying ω_s in order to determine whether the interface remains bound or undergoes a reentrant transition to the unbound state we must identify whether or not q_3 will exceed the value of q_1. We have determined this numerically within the triple parabola model. The value of q_3 is found to increase in the vicinity of $\tilde{\tau}=0$ as $|\mu_s|$ is increased. In contrast q_1 rapidly decreases as $|\mu_s|$ is increased. Thus as $|\mu_s|\to\infty$ the ratio $q_3/q_1\to\infty$ so that for sufficiently large (fixed) $|\mu_s|$ there will be no transition and the interface will always be bound. For smaller fixed $|\mu_s|$ but still in the mean-field critical region one may cross two transition lines enclosing a region representing an unbound interface as ω_s is varied. We remark that the ''renormalization'' of q_1 due to the inclusion of a nonzero q_2 term discussed in Sec. III does not effect the above conclusion since q_2 is found to have the same qualitative behavior as q_1.

To complete the renormalized phase diagram we must explore the effect of fluctuations on the mean-field first-order phase boundary. This may be achieved in much the same way as we examined the critical transition in earlier sections with a slightly different modified bare potential. Near the first-order transition, the coefficient w_{020} in the expansion (2.2) for the potential is negative and so it is necessary to take the next order term into account. Furthermore, the coefficients s_{020} and s_{021} in the stiffness expansion (2.3), along with the corresponding coefficients in Eq. (2.4) for the rigidity, will both change sign at the tricritical point in Fig. 1. Thus, instead of Eq.(3.5), we need to consider the following modified bare potential

$$\tilde{W}^{(0)}(l)=\tilde{\tau}(1-q_1 l)e^{-l}+(q_3 l-r)e^{-2l}+se^{-3l}, \quad (5.1)$$

with $\tilde{\tau}$, q_1, q_3, and r as before [see Eq. (3.3)], while $s=w_{110}+c_1 s_{110}+c_2 k_{110}>0$. In this formulation the final two terms (i.e., re^{-2l} and se^{-3l}) are only required to ensure that $l=0$ is not incorrectly identified as a boundary minimum of the potential. As in Sec. III, we can gauge the effect of fluctuations by performing a mean-field-like study of this potential. The role played by q_1 is again intriguing, since it changes the sign of the leading order term in the potential. By minimizing Eq. (5.1) it is straightforward to identify a second-order unbinding transition as $\tilde{\tau}\to 0^+$, which we may interpret as a fluctuation-induced critical transition. By further decreasing $\tilde{\tau}$, the interface becomes bound again at a first-order transition, pointing to reentrant behavior, compatible with the aforementioned results for the bare critical transition. These results are also found from the fully linearized RG study in regimes I and II, where in each case the divergence of l at the second-order transition is identical to that found for the * transition in the relevant regime.

Thus combining all of our results yields a renormalized surface phase diagram as depicted in Fig. 6. We observe that

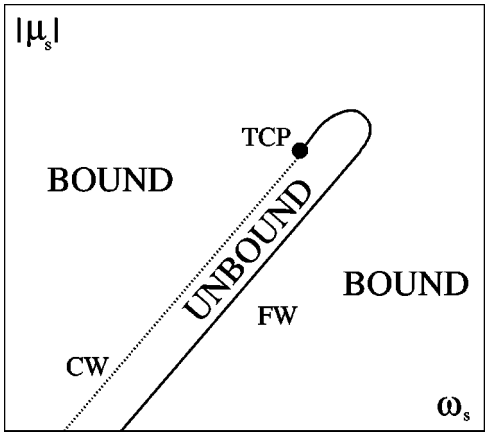

FIG. 6. Schematic phase diagram for the unbinding of a wall-microemulsion interface including the effect of fluctuations. The unbound state is stable only in a narrow region confined by critical (dotted) and first-order (solid) phase transition lines. The filled circle indicates the tricritical point (TCP).

the unbound state is stable only in a limited region of the diagram and that it is no longer the case that unbinding transitions are found for all values of the surface parameters. Note that the original large unbound region in the high $|\mu_s|$ regime of Fig. 1 has become a region of bound states, which is directly attributable to the presence of the q_1 term in the renormalized potentials. The phase transition lines that are the borders of the unbound region in Fig. 6 follow from the renormalization of the mean-field phase boundaries as outlined above. We distinguish a critical transition CW (dashed line) and a first-order transition FW (solid line) merging at a tricritical point. In regime I the TCP is located at the same position as the TCP in the mean-field phase diagram, whereas in regime II it may shift depending on whether or not $q_3 > Q_3$ [see Eq. (4.31)] near the mean-field TCP. Our calculation is insufficient to provide a quantitative measure of the width of the unbound region in the surface phase diagram although we anticipate it is rather narrow. More importantly there is no longer a prescriptive route for finding the unbinding transition in the system once fluctuation effects have been included. For example, if in a given system we find the interface is in a bound state, it is not certain that by varying the surface field, say, that we could induce an unbinding transition. Even if it is possible we would not be able to deduce *a priori* whether the field should be increased or decreased. Hence we believe that the opportunity for observing an unbinding transition is severely reduced due to fluctuation effects.

VI. CONCLUSIONS

In this paper we have analyzed the effect of fluctuations upon the unbinding of a water-microemulsion interface from a substrate in a confined complex fluid. At mean-field level such a transition is predicted for all values of the surface parameters as shown in Fig. 1; in particular, for any given enhancement a transition can be induced by varying the surface field. We have demonstrated that this is *not* generally true beyond mean-field due to the presence of position-dependent contributions in the interfacial stiffness and rigidity. A detailed RG analysis reveals that the surface phase diagram is dramatically revised due to fluctuations, with Fig. 1 being replaced by Fig. 6. Most notably the unbound region in the phase diagram is rather limited and so any observation of the unbinding transition would require a fine tuning of the surface parameters. Furthermore, for a given surface enhancement it is no longer guaranteed that we could induce a transition by varying the surface field $|\mu_s|$. As a consequence we believe that the observation of such a transition in a simulation would prove problematic and thus suggest that this system would be a poor candidate for observing the predicted nonuniversal critical exponents associated with unbinding [19].

We comment that the effect of the position-dependent contributions in the gradient coefficients is significantly different to the previously predicted stiffness instability mechanism for fluids [15,21]. In that case a second-order transition is destabilized by new next-to-leading-order terms in the renormalized interface potential. In the present case it is the leading order term that is modified, yielding the dramatic changes in phase behavior described above. It is opportune at this stage to comment that recent extensions to interface modeling for simple fluids could also be applied to ternary mixtures and can be relevant if one is interested in extending the analysis beyond the calculation of the phase diagram. In particular, when considering a complete unbinding transition it may be appropriate to derive a two-field interface model incorporating one interface that remains bound to the wall, and one that unbinds in the limit of the transition [32]. This extended model would contain both a stiffness matrix familiar from simple fluids and a curvature matrix. An interesting line of future research would be to examine whether one finds a connection between these matrices and the free-energy, analogous to the stiffness matrix–free-energy relation of simple fluids [33,34].

Finally, we note that the RG results described in Secs. III and IV are very general and so this analysis is expected to be applicable to a range of unbinding behavior in ternary mixtures. The overall results will depend sensitively on the sign of the coefficients q_1, q_3, etc., appearing in the modified bare potential [see Eq. (3.4)]. For example a bare critical transition is predicted to remain continuous if q_1 and q_3 are negative, very different to the behavior in our specific system where q_1 and q_3 are both positive. Thus while we have demonstrated that the unbinding of the water-microemulsion interface from a substrate is inhibited due to fluctuation effects, the same RG analysis may support mean-field predictions for other unbinding transitions.

ACKNOWLEDGMENTS

This research was supported by the EPSRC, U.K. (GR/N37070) and the Nuffield Foundation (NUF-NAL 99).

APPENDIX: GENERAL SOLUTION OF THE RG FLOW EQUATIONS

In this Appendix we show how the RG flow equations (2.14)–(2.17) can be solved in closed form for general dimension d.

To start, it is convenient to note that we can decouple the set of partial differential equations by defining

$$U^{(t)}(l)=W^{(t)}(l)+f_1(t)\Delta\Sigma^{(t)}(l)+f_2(t)\Delta\kappa^{(t)}(l), \tag{A1}$$

where the functions $f_1(t)$ and $f_2(t)$ are given by

$$f_1(t)=-\Omega\Lambda^2 e^{(d-1)}\int_0^t ds\,\frac{e^{-(d-1)s}}{\Sigma_\infty+\kappa_\infty\Lambda^2 e^{-2s}} \tag{A2}$$

and

$$f_2(t)=-\Omega\Lambda^4 e^{(d+1)}\int_0^t ds\,\frac{e^{-(d+1)s}}{\Sigma_\infty+\kappa_\infty\Lambda^2 e^{-2s}}. \tag{A3}$$

With these definitions $U^{(t)}(l)$ satisfies the equation

$$\frac{\partial U^{(t)}(l)}{\partial t}=(d-1)U^{(t)}(l)+\zeta l\frac{\partial U^{(t)}(l)}{\partial l}+\frac{\Omega}{\Sigma_\infty+\kappa_\infty\Lambda^2 e^{-2t}}\frac{\partial^2 U^{(t)}(l)}{\partial l^2}. \tag{A4}$$

This equation is analogous to the original wall-potential flow equation solved by Fisher and Huse [19], thus we may readily identify the solution

$$U^{(t)}(l)=\frac{e^{(d-1)t}}{\sqrt{2\pi}g(t)}\int_{-\infty}^{\infty}dl'\,U^{(0)}(l')\exp\left[-\frac{(e^{\zeta t}l-l')^2}{2g^2(t)}\right]. \tag{A5}$$

The width of the convolution $g(t)$ is given by

$$g^2(t)=2\int_0^t ds\,\frac{\Omega e^{2\zeta s}}{\Sigma_\infty+\kappa_\infty\Lambda^2 e^{-2s}}. \tag{A6}$$

It is also evident that the solutions for the stiffness and the rigidity will have similar forms [compare Eqs. (2.14) and (2.15) to (A4)]. All we need to do is replace U by $\Delta\Sigma$ or $\Delta\kappa$, and $d-1$ by 0 or -2, respectively. Thus, the solutions read

$$\Delta\Sigma^{(t)}(l)=\frac{1}{\sqrt{2\pi}g(t)}\int_{-\infty}^{\infty}dl'\,\Delta\Sigma^{(0)}(l')\exp\left[-\frac{(e^{\zeta t}l-l')^2}{2g^2(t)}\right] \tag{A7}$$

and

$$\Delta\kappa^{(t)}(l)=\frac{e^{-2t}}{\sqrt{2\pi}g(t)}\int_{-\infty}^{\infty}dl'\,\Delta\kappa^{(0)}(l')\exp\left[-\frac{(e^{\zeta t}l-l')^2}{2g^2(t)}\right]. \tag{A8}$$

It is now straightforward to find the solution for the binding potential since $W^{(t)}(l)=U^{(t)}(l)-f_1(t)\Delta\Sigma^{(t)}(l)-f_2(t)\Delta\kappa^{(t)}(l)$ from Eq. (A1). Thus

$$W^{(t)}(l)=\frac{e^{(d-1)t}}{\sqrt{2\pi}g(t)}\int_{-\infty}^{\infty}dl'\,\tilde{W}^{(0)}(l')\exp\left[-\frac{(e^{\zeta t}l-l')^2}{2g^2(t)}\right], \tag{A9}$$

where the initial potential is

$$\tilde{W}^{(0)}(l)=W^{(0)}(l)-f_1(t)e^{-(d-1)t}\Delta\Sigma^{(0)}(l)-f_2(t)e^{-(d+1)t}\Delta\kappa^{(0)}(l). \tag{A10}$$

In $d=3$ we may explicitly solve the integrals (A2) and (A3) so that Eq. (A10) reduces to Eq. (2.22). Moreover, in three dimensions $\zeta=0$ and so Eq. (A9) reduces to Eq. (2.21).

[1] G. Gompper and M. Schick, in *Phase Transitions and Critical Phenomena*, edited by C. Domb and J.L. Lebowitz (Academic, London, 1994), Vol.16, and references therein.
[2] B. Widom, Langmuir **3**, 12 (1987).
[3] G. Gompper and M. Schick, Phys. Rev. Lett. **65**, 1116 (1990).
[4] F. Schmid and M. Schick, J. Chem. Phys. **102**, 7197 (1995).
[5] K.V. Schubert and R. Strey, J. Chem. Phys. **95**, 8532 (1991).
[6] G. Gompper and M. Kraus, Phys. Rev. E **47**, 4289 (1993).
[7] G. Gompper and S. Zschocke, Phys. Rev. A **46**, 4836 (1992).
[8] C.J. Boulter and F. Clarysse, Phys. Rev. E **60**, R2472 (1999).
[9] F. Clarysse and C.J. Boulter, Physica A **278**, 356 (2000); **289**, 607 (2001).
[10] F. Clarysse and C.J. Boulter, Fluid Phase Equilibria (to be published).
[11] For a general review of wetting, see S. Dietrich, in *Phase Transitions and Critical Phenomena*, edited by C. Domb and J.L. Lebowitz (Academic, London, 1988), Vol. 12.
[12] R. Lipowsky, D.M. Kroll, and R.K.P. Zia, Phys. Rev. B **27**, 4499 (1983).
[13] E. Brézin, B.I. Halperin, and S. Leibler, Phys. Rev. Lett. **50**, 1387 (1983).
[14] R. Lipowsky and S. Leibler, Phys. Rev. Lett. **56**, 2541 (1986).
[15] M.E. Fisher and A.J. Jin, Phys. Rev. Lett. **69**, 792 (1992).
[16] M.E. Fisher, A.J. Jin, and A.O. Parry, Ber. Bunsenges. Phys. Chem. **98**, 357 (1994).
[17] In some cases, a thin-thick transition may be found in the vicinity of TCP preceding the wetting transition and leading to additional critical points [8–10]. However, surface transitions of this kind are not of primary relevance in the present paper.
[18] For a review of RG methods applied to interface behavior, see G. Forgacs, R. Lipowsky, and Th.M. Nieuwenhuizen, in *Phase Transitions and Critical Phenomena*, edited by C. Domb and J.L. Lebowitz (Academic, London, 1991), Vol. 14.
[19] D.S. Fisher and D.A. Huse, Phys. Rev. B **32**, 247 (1985).
[20] A.J. Jin and M.E. Fisher, Phys. Rev. B **47**, 7365 (1993).
[21] A.J. Jin and M.E. Fisher, Phys. Rev. B **48**, 2642 (1993).
[22] C.J. Boulter, Phys. Rev. Lett. **79**, 1897 (1997); Phys. Rev. E **57**, 2062 (1998).

[23] Due to the symmetry in the Ginzburg-Landau theory between the oil-rich and water-rich phases, analogous results are found if we chose $\mu_s > 0$. However, as discussed in Ref. [9], it is most reasonable on physical grounds to take $\mu_s < 0$ corresponding to a preference for the water phase, since when the adsorbed phase is the oil-rich one, long-range forces will always suppress the unbinding transition.
[24] G. Gompper and M. Hennes, J. Chem. Phys. **102**, 2871 (1995).
[25] F. Clarysse. Ph.D. thesis, Leuven, 2000.
[26] R. Lipowsky and M.E. Fisher, Phys. Rev. Lett. **57**, 2411 (1986).
[27] R. Lipowsky and M.E. Fisher, Phys. Rev. B **36**, 2126 (1987).
[28] G. Gompper and D.M. Kroll, Europhys. Lett. **5**, 49 (1988); Phys. Rev. B **37**, 3821 (1988).
[29] H. Chaar, M.R. Moldover, and J.W. Schmidt, J. Chem. Phys. **85**, 418 (1986).
[30] M.E. Fisher and H. Wen, Phys. Rev. Lett. **68**, 3654 (1992).
[31] R. Evans, D.C. Hoyle, and A.O. Parry, Phys. Rev. A **45**, 3823 (1992).
[32] C.J. Boulter and A.O. Parry, Phys. Rev. Lett. **74**, 3403 (1995).
[33] A.O. Parry and C.J. Boulter, Mol. Phys. **87**, 501 (1996).
[34] C.J. Boulter and A.O. Parry, J. Phys.: Condens. Matter **9**, 7003 (1997).